Progress In Electromagnetics Research B, Vol. 100, 73–89, 2023

Estimation of Thickness and Dielectric Characteristics of Sea Ice from Near-Field EM Measurements Using Deep Learning for Large Scale Polar Ice Probing

Mohammad S. Islam[1, *], Sadman Shafi[1], and Mohammad Ariful Haque[2]

Abstract—The near and far field EM responses over layered media have long been exploited in diversified applications such as remote sensing, monitoring, and communication. In this work, we utilize the near field dependence of the EM fields of a three layered structure resembling air-sea ice-sea water to estimate the thickness and dispersion characteristics of sea ice using deep learning technique. We explore two key methods of field measurement termed as the fixed and scaled sweep methods. In the fixed radial sweep method, the receiver distance and height from the source are kept constant, and in the scaled sweep method both the receiver distance and height are set as a scaled function of the operating wavelength. A synthetic training dataset has been generated (using analytical computation and FEM simulation) in the low MHz band, which is used to train a deep learning model. The model is tested on different test datasets with frequencies inside, below and above the training limits. Even though the fixed sweep method is simpler to implement, the scaled sweep appears to perform better across the wide range of test frequency, both in and outside the training range. When the test frequency is inside the training range, the percentage errors for thickness, dielectric constant, and loss tangent were found to be $< 2\%$, $< 10\%$, and $< 5\%$, respectively, for the fixed radial sweep, whereas for the scaled sweep the percentage error is $< 1\%$ for all three measurement parameters. When the test frequency deviates further from the training range, the percentage error gradually increases. Later, we investigate the problem of determining sea ice thickness assuming a priori knowledge of sea ice dielectric parameters, and results show that the model estimates the thickness of the sea ice bulk with error as low as 0.1%.

1. INTRODUCTION

The effect of electromagnetic fields in the presence of layered dielectric systems has been of interest for many years, with a diversified domain of applications. The applications range from determining the dimensions (size, thickness) of various geophysical [1–6] and biological systems [7–9], identification of the location and shape of buried objects [10–12], to the effect of layered dielectrics to tamper electromagnetic field response over various radiating systems such as different types of antennas [13–18]. In the analytical treatment of the electromagnetic field response, these layered systems are often represented as planar inhomogeneous dielectric structures. These dielectric layers, as a whole, are termed differently depending on the application. For example, when the dielectric system resembles a geophysical or biological system, the layers are often termed as 'subsurfaces', and the application generally involves measuring the thickness of each subsurface and detecting the presence of inhomogeneity within these subsurfaces [1, 2, 6, 11]. On the other hand, when the layered dielectric system is used to manipulate electromagnetic fields for radiation enhancement (such as gain enhancement of antennas), the layers are termed as 'substrates' [17–19]. However, more often than not, these terms can be used interchangeably.

Received 20 December 2022, Accepted 13 May 2023, Scheduled 20 May 2023
* Corresponding author: Mohammad Shifatul Islam (shifatul@anyeshan.com).
[1] Anyeshan Limited, Bangladesh. [2] Department of Electrical and Electronic Engineering, Bangladesh University of Engineering and Technology, Bangladesh.

Particular attention has been given for specific dielectric systems where the number of layers is three, as numerous geophysical, environmental, and antenna systems are often modelled as simplified planar three layered media [1–6, 8, 20, 21]. For geophysical probing applications, the upper media is often air. The middle layer (which is the subsurface) is a lossy dielectric whose thickness and inhomogeneity measurement is often the main interest. The bottom layer is a semi-infinite halfspace, which terminates the three layered systems. Electromagnetic fields are used to probe the subsurface in many ways. One old and widely used method is called "Radio interferometry" [1, 2], where a radiating source is placed on the upper air-subsurface interface and operated at a wavelength smaller than the dimensions (thickness) of the subsurface. From the reflected field response and the relative location of the peaks and troughs, one can estimate the subsurface properties. The sharpness of these extremes also yields crucial information on the subsurface dielectric loss, and in general, the more the dielectric loss is, the damper the peaks and troughs become [2]. Another type of subsurface probing method involves the use of electromagnetic pulses using various forms of Radars where the time delay and magnitude of the reflected pulses provide necessary information on the subsurface or any further anomalies buried under it [10–12]. For these applications, the operating wavelength is also a few orders less than the subsurface dimensions, so that the reflected pulses can travel multiple wavelength distance before reaching the receiver.

From the analytical treatment of the radio interferometry [2], it is found that this method is not suitable for determining the properties of subsurface when its thickness is very small compared to the wavelength, and when the loss is several orders higher. For this case, interference patterns diminish very quickly. For such types of dielectric configurations, the authors [20] proposed an idea of "near field interferometry" using ideal dipole antennas, where an analytical study of near field magnetic fields shows clear monotonic dependence with both thickness and dielectric properties of the subsurface, whose thickness is in the subwavelength regime. The study was progressed further in [22], where the analytical results were verified using a finite element model, with the additional exploration of the electric field dependencies. It was shown that electric fields showed a stronger and more nonlinear dependence on thickness, and showed distinctive maxima when the field values are measured very close to the top interface. The study also showed that the positions of those extremes were directly related to the thickness and the dielectric constant of the subsurface.

The inverse relation between the subsurface parameters (dimension and dielectric properties) and measured EM field data is very complicated, and no approximate or closed form solution is attainable. So instead of defining an inverse function, radio interferometry tries to estimate the subsurface parameters from the interference patterns and field magnitudes. This estimation is not simultaneous, and one needs to have a priori knowledge of the subsurface dielectric properties to estimate the thickness and vice versa [2]. On the other hand, if it were possible to formulate an exact mathematical relation between the field values with the dimension and dielectric properties of the subsurface, a simultaneous estimation of these two parameters might be a possibility. To solve similar geophysical inverse scattering problems, where closed form inverse relation between the scatterer properties and measured variables is very hard or impossible to obtain, the use of deep neural networks (DNN) [23, 24] has recently gained a lot of attention and has become a trend in several works [25–29]. [29] tried to estimate all of the subsurface parameters from the near field data using deep learning over different planar three layered structures. The work demonstrated that a simultaneous estimation is indeed theoretically possible for more than one layer of subsurface using simplified deep learning regression models. Though the estimation performance degraded with more layers and with the addition of different levels of noise, the introduction of deep learning for the particular inverse problem also appears quite promising.

Among different three layered systems, the most abundant in nature are systems where the bottom layer (ground) is composed of a highly reflective material [1, 3, 20, 22]. For such layered systems it has been shown that in the subwavelength dimensions, the resolution of EM fields with subsurface parameters is very significant compared to other three layered dielectric systems; therefore, it offers a better inverse estimation performance [29]. This observation motivated us to apply near field EM measurement method to characterize sea ice bulks floating over very lossy sea water [30]. In comparison with the linear subsurface materials in [29], sea ice has a more lossy and nonlinear dispersion [31–33], relation [4, 6, 31, 34], which is primarily attributed to the presence of saline brine packets trapped inside the sea ice bulk. Hence, the characterization of sea ice can be more challenging in comparison to

subsurfaces with a more linear dispersion relation.

In the literature, there exist methods which can measure sea ice dielectric properties from collected sample ice data [31–35] and thickness [36–43] independently with or without electromagnetic waves. Among these methods, EM sounding [43] is a well-known technique for measuring sea ice thickness, which uses a transmitter and a receiver coil. The transmitter-sea water interaction induces a secondary field in the receiver coil, and it exploits the theoretical relationship between the received field strength and sea-ice thickness. The relationship is expressed as a complex integral representation with a Bessel function of the first kind of order zero, which can be solved numerically to estimate the thickness for given conductivities of the ice and water.

In our work, we present a novel method of simultaneous estimation of both sea ice thickness and dielectric properties using DNNs, which could open up a completely new paradigm in large scale monitoring of polar marine environment. Unlike the traditional probing using high frequency EM waves and pulses, we propose a low frequency measurement technique to overcome the dimension constraints for large, lossy media. The DNN is trained on near field data with a defined range of low frequencies so that the thickness of sea ice falls in the subwavelength dimensions. In addition to characterizing sea ice from low frequency measurements, we also explore the frequency mismatch between the training and test data. In other words, we want to determine the possibility of characterizing sea ice parameters even when the range of frequencies at inference time is different from those in the training dataset. If this is a plausible case, we can actually train a deep learning model with a limited training dataset and use this model to characterize sea ice over a wide range of experimental frequencies. We will present the results in a later section and show that the idea is feasible if we define the measurement method in a wavelength scaled way.

We divide the rest of the paper into three sections. In Section 2, we present the air-sea ice-sea water system and discuss the physics behind the feasibility of estimating sea ice thickness and dielectric properties. In Section 3, we provide two measurement schemes termed as fixed and scaled radial sweep methods to obtain the field dataset. We also describe the deep learning model which learns the thickness and inherent dispersion relation of sea ice from the field measurements. In Section 4 we present the performance of the deep learning model to characterize sea ice, with a qualitative comparison between the two measurement schemes, and discuss some possible limitations and scope for improvement of the near field measurement method. Finally, the results and our findings are summarized in Section 5.

2. THREE LAYERED AIR-SEA ICE-SEA WATER MEDIA

In this section, we present a mathematical and physical interpretation of the EM field response of an air-sea ice-seawater environment [43] and describe how the field responses are related to the characterization parameters. As shown in Fig. 1, we consider a Hertzian electric dipole as the source of EM radiation. We label air, sea ice, and seawater as layers 0, 1, and 2, respectively. Each layer has a complex dielectric constant of $\epsilon_{c,m}$, which consists of a real polarization component ϵ_m and an imaginary loss component $\tan\delta_m$ through the following relation:

$$\epsilon_{c,m} = \epsilon_m(1 + i\tan\delta_m), \text{ where } m = 0, 1, 2$$

where $i = \sqrt{-1}$. The EM fields depend on the "generalized plane wave reflection coefficient" [20] of the three layered system, which in turn is a function of the thickness and dielectric properties of the subsurface (i.e., sea ice). The expression of the total reflection coefficient for the three layered system is [44]

$$\widetilde{R}_{0,1} = \frac{R_{0,1} + \widetilde{R}_{1,2}\, e^{2ik_{z,1}d}}{1 + R_{0,1}\widetilde{R}_{1,2}\, e^{2ik_{z,1}d}} \tag{1}$$

Here, the tilde superscript over the reflection coefficient denotes the total generalized reflection, which considers the reflection from all the layers below. The reflection coefficients without tilde superscript indicate the "Fresnel reflection coefficient" between the two successive layers [45]. The propagation constant in each media is k_m, and its component along the direction of stratification is $k_{z,m}$, for $m = 1, 2$. The component tangential to the surface boundaries is k_t, and d is the thickness of subsurface (sea ice). Dipole sources excite spherical waves, which can be decomposed into a tangential cylindrical

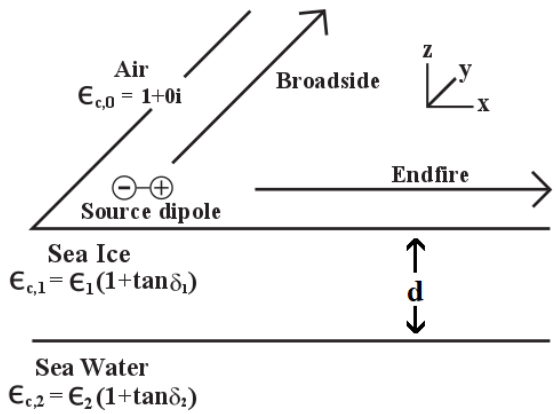

Figure 1. Schematic diagram of the three layered air-sea ice-seawater environment, with stratification along the negative z axis. The air and the sea water layers are semi infinite, and the sea ice layer has a finite thickness d. A Hertzian dipole source is placed on the top of the air-sea ice interface, with the endfire direction defined as the direction of the dipole axis (x axis), and the broadside direction defined as the direction orthogonal to the dipole axis (y axis).

wave component [46] and a planewave component along the direction of the stratification. Therefore, $k_t = k_\rho$ [44], and $k_m = \sqrt{k_\rho^2 + k_{z,m}^2}$. Throughout the paper, we have chosen an $e^{-i\omega t}$ time dependence, and therefore for choosing the appropriate square roots in all the following equations, we have taken the value which has positive real and imaginary components to satisfy the radiation condition. For the source medium (air or medium 0), we omit the m subscripts from the propagation components to avoid congestion in the field expressions. That is, in the source region, the propagation constant and the component along stratification are k and k_z, respectively.

2.1. Physics behind the Concept of Simultaneous Estimation of Thickness and Dielectric Properties of Sea Ice

We manipulate the expression of the reflection coefficient presented in (1) to understand the motivation behind our proposed concept of thickness and dielectric estimation of the subsurface (sea ice). First, we represent the term $2ik_{z,1}d$ in (1) in the angular representation [44]. Assuming $|\epsilon_{c,1}| \gg 1$, we can write:

$$2ik_{z,1}d = 2id\sqrt{k_1^2 - k_\rho^2} = \frac{4\pi id}{\lambda}\sqrt{\epsilon_{c,1} - \sin^2\theta} \approx \frac{4\pi id}{\lambda}\sqrt{\epsilon_{c,1}} = g(\sqrt{\epsilon_{c,1}}d)$$

where $\theta = \arctan\frac{k_\rho}{k_z}$ is the angle of incidence, which can be either real or complex. The reflection coefficient R can be either TE or TM mode. However, irrespective of the mode, since the ground (sea water) is highly conductive, the bottom layer will always have reflection coefficient $R_{1,2} \approx \widetilde{R_{1,2}} \approx \pm 1 = e^{\pm i\pi}$ [47]. Now, for TM case, the expression of the Fresnel reflection coefficient between media 0 and 1 (air and sea ice) is [44]:

$$\begin{aligned} R_{0,1}^1 &= \frac{\epsilon_{c,1}k_z - \epsilon_0 k_{z,1}}{\epsilon_{c,1}k_z + \epsilon_0 k_{z,1}} = \frac{\epsilon_{c,1}\sqrt{\epsilon_0 - \sin^2\theta} - \epsilon_0\sqrt{\epsilon_{c,1} - \sin^2\theta}}{\epsilon_{c,1}\sqrt{\epsilon_0 - \sin^2\theta} + \epsilon_0\sqrt{\epsilon_{c,1} - \sin^2\theta}} \\ &= \frac{\epsilon_{c,1}\cos\theta - \sqrt{\epsilon_{c,1} - \sin^2\theta}}{\epsilon_{c,1}\cos\theta + \sqrt{\epsilon_{c,1} - \sin^2\theta}} = f_1(\sqrt{\epsilon_{c,1}}) \end{aligned} \tag{2}$$

and for TE waves [44]:

$$R_{0,1}^{2} = \frac{\mu_1 k_z - \mu_0 k_{z,1}}{\mu_1 k_z + \mu_0 k_{z,1}} = \frac{\cos\theta - \sqrt{\epsilon_{c,1} - \sin^2\theta}}{\cos\theta + \sqrt{\epsilon_{c,1} - \sin^2\theta}} = f_2(\sqrt{\epsilon_{c,1}}) \tag{3}$$

Thus, we can rewrite (1) as follows:

$$\widetilde{R_{0,1}^{j}} = \frac{f_j(\sqrt{\epsilon_{c,1}}) + e^{g(\sqrt{\epsilon_{c,1}}d)\pm i\pi}}{1 + f_j(\sqrt{\epsilon_{c,1}})e^{g(\sqrt{\epsilon_{c,1}}d)\pm i\pi}} \tag{4}$$

with $j = 1, 2$ representing TM and TE reflection coefficients, respectively. From (4), it is evident that both TM and TE reflection coefficients are functions of medium thickness and the dielectric property. Comparing (2) and (3) with (4), we also find that the TM reflection is a strong function of both $\epsilon_{c,1}$ and d, and TE reflection is a weaker function of $\epsilon_{c,1}$ but a strong function of d. Now, the idea behind the simultaneous estimation of thickness and dielectric constant of sea ice is that we excite a source which has both TM (a strong function of $\epsilon_{c,1}$ and d) and TE (a strong function of d) components. A combined knowledge of both field components would enable the separation of the two constituent parameters through a convenient regression of arbitrary complexity. The choice of using a horizontal source dipole therefore is the perfect choice as it excites both field modes.

Even though the mathematical reasoning is plausible, there are some difficulties in simultaneously estimating the thickness and dielectric properties. Since the dielectric constant and thickness appear as a product term ($\sqrt{\epsilon_{c,1}}d$) in (4), an error in measuring thickness should contribute to the erroneous estimation of dielectric constant to a certain degree, and vice versa. Furthermore, the complex and nonlinear nature of $\epsilon_{c,1}$ with frequency makes the task of estimating the parameter more challenging.

We have chosen the frequency of operation in the MHz range as sea ice works as a partially transparent medium at this frequency range. The feasibility of the whole method depends on the fact that the air-sea ice interface will produce a partial reflection, and the sea ice-seawater interface will produce a total reflection; the combination of them will suppress the source field and provide information on the medium characteristics. The choice of the MHz frequency is convenient for two reasons.

- For lower frequencies, sea ice bulks have a very large dielectric constant [31, 32, 35], which results in almost total reflection from the top interface, and very few waves will leak through the bulk, which will result in a very low resolution in measurement performance.
- As sea ice bulk has a moderately high dielectric loss, a higher frequency would mean a larger propagation loss. Hence, the penetrating waves will attenuate very quickly inside the sea ice bulk before reflecting back to the receiver, and therefore there would be no information of the depth of sea ice.

Before getting into the methodology section, we provide a physical interpretation to estimate the variation of field magnitudes with changing thickness and dielectric constant of the sea ice. Since the

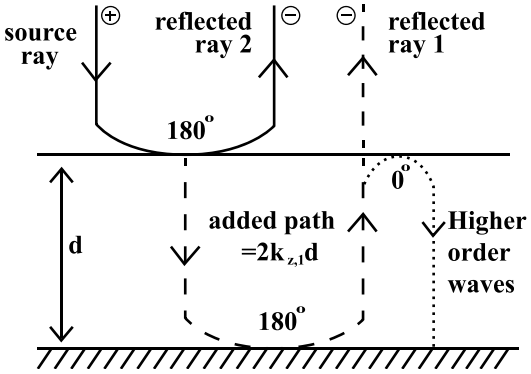

Figure 2. Physical interpretation of the variation of field magnitudes with changing thickness and dielectric constant of the lossy subsurface (i.e., sea ice) using ray optics diagram [44].

bottom seawater layer is highly conductive, it will reflect almost all the waves from the sea ice-seawater interface (ray 1) as shown in Fig. 2. Another wave reflection will come from the air-sea ice interference (ray 2). With respect to the source, both of these reflected waves are in opposite phase and will always try to cancel the source ray for subwavelength thickness. Hence, the magnitude of the total fields will be lower. The more opposite in the phase the combined rays 1 and 2 are with respect to the source, the lower the total field response will be.

2.2. Relation with d

When the thickness is low, ray 1 will travel less path from the bottom interface to the receiver point; therefore at the receiver, ray 1 will be more "out of phase" to the source, which will suppress the source field more, and the total field will be lower. When the thickness is large, ray 1 will travel a longer path and therefore will be less "out of phase" compared to the source. In addition, the propagation inside a lossy sea ice bulk will degrade the magnitude of the reflected waves to some extent. This will result in a much weaker reflected wave opposing the phase of the source, and the cancellation will be smaller. So the total field response will be larger at large thickness values of sea ice and smaller for small thickness values of sea ice. As shown in Fig. 3(a), this effect is more pronounced with the TE waves, which strongly depend on the thickness.

2.3. Relation with ϵ_1 and tanδ_1

The larger the value of ϵ_1 is, the larger the reflection will be from the top interface (ray 2), and the more the reflected waves will cancel out the source. So the total field response will be lower. In the same token, the lower the value of ϵ_1 is, the lower the reflection is from the top interface, and the larger the response of the field values is. Addition of the medium loss will contribute not just to the reflection magnitude, but also to the phase of the top surface of the reflection coefficient, which will affect the reflection characteristics. In general, the higher the magnitude of $\tan\delta_1$ is, the more the reflection is from the top surface, and the lower the total field will be. The phenomenon is more prominent in the TM reflections, which is a strong function of both the thickness and the dielectric properties of the sea ice bulk (see Fig. 3(b)).

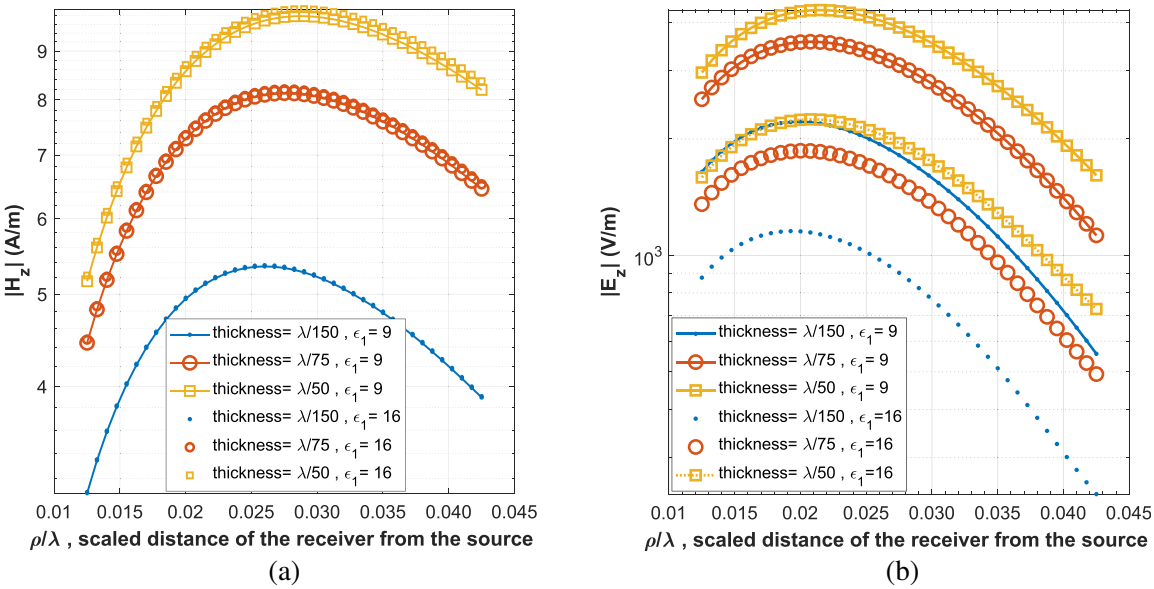

Figure 3. Variation of TE and TM mode fields with radial distance of the receiver from the source for different thickness and dielectric constants of the subsurface. The solid lines are for $\epsilon_1 = 9$, and the dotted lines are for $\epsilon_1 = 16$. Fig. 3(a) shows strong dependency of H_z on thickness and Fig. 3(b) shows strong dependency of E_z on both thickness and dielectric constant.

3. METHODOLOGY

In this section, we will discuss the method by which the thickness and dielectric properties of sea ice can be estimated from the dipole radiated field values. As stated earlier, we will consider the air-sea ice-seawater system as a planar, three layered stratified system, and the frequency will be in the MHz range. We choose to solve the inverse problem of estimating the thickness and dielectric properties using a deep learning model, which needs sufficient data to train and later to test the performance of the model. The training data is generated using both an analytical method and a finite element (FEM) simulation. We use analytical data to describe the feasibility of solving such an inverse problem from a theoretical perspective. In addition, due to the ease of computation, we are also able to generate an enormous amount of data using analytical method, so that the model will always be very well trained, and the results would be clearly interpreted and understood. On the other hand, FEM simulation data is more representative of practically acquired data, which should be much less in quantity. The FEM simulation environment is generated using COMSOL Multiphysics [48], a physics simulation software. Due to the relatively large computation time, the amount of generated data is much less than those in the analytical methods, and therefore the model is likely to be overfitted on the training data. For the FEM modeling, we choose the meshing to be relatively coarse, just enough so as the integrity of the data is maintained, therefore ensuring a faster computation as a tradeoff and generating a reasonable amount of data.

We describe the method of solving the inverse problem of sea ice thickness in three steps. First, we will define the three layered air-sea ice-sea water environment, then we will generate field data for training and testing over a band of frequencies, and finally, we will use the dataset to train a deep learning network capable of solving the inverse problem of simultaneous estimation of the thickness and dispersion relations of sea ice.

3.1. Modelling of the Three Layered System

The top layer (air) is the simplest to model, with a fixed dielectric constant of $\epsilon_0 = 1$, and loss tangent $\tan\delta_0 = 0$. For modeling the sea ice bulk, we have used the dispersion curves presented in [33]. The dispersion of sea ice is a direct function of temperature, frequency, and salinity of the ice sample. Due to the exponential and monotonic dispersion relation in the low MHz ranges, we have used linear interpolation to estimate the dielectric constants at different temperature and salinity values.

The dielectric modeling of seawater is available in [30, 49], where the dispersion of the sea water sample is fitted into a Debye model as follows:

$$\epsilon_{c,2} = \epsilon_{inf} + \frac{\epsilon_s - \epsilon_{inf}}{1 + i\omega\tau_s} - \frac{i\sigma_s}{\omega\epsilon_0}; \tag{5}$$

Here,

$$\begin{aligned}
\epsilon_{ref} &= 87.134 - 1.949\times10^{-1}T - 1.276\times10^{-2}T^2 + 2.491\times10^{-4}T^3\\
\sigma_{ref} &= S(0.182521 - 1.46192\times10^{-3}S + 2.09324\times10^{-5}S^2 - 1.28205\times10^{-7}S^3)\\
\tau_{ref} &= 1.768\times10^{-11} - 6.086\times10^{-13}T + 1.104\times10^{-14}T^2 - 8.111\times10^{-17}T^3\\
\alpha &= 1 + 1.613\times10^{-5}ST - 3.656\times10^{-3}S + 3.210\times10^{-5}S^2 - 4.232\times10^{-7}S^3\\
\epsilon_s &= \epsilon_{ref}\alpha\\
\Delta &= 25 - T\\
\beta &= 2.033\times10^{-2} + 1.266\times10^{-4}\Delta + 2.464\times10^{-6}\Delta^2\\
&\quad -S(1.849\times10^{-5} - 2.551\times10^{-7}\Delta + 2.551\times10^{-2}\Delta^2)\\
\sigma_s &= \sigma_{ref}\exp(-\Delta\beta)\\
\gamma &= 1 + 2.282\times10^{-5}ST - 7.638\times10^{-4}S - 7.760\times10^{-6}S^2 + 1.105\times10^{-8}S^3\\
\tau_s &= \tau_{ref}\gamma\\
\epsilon_{inf} &= 4.9
\end{aligned}$$

where T is the temperature in °C, and S is the salinity in ppt (parts per thousand).

3.2. Description of the Environment and Dataset

For the hypothetical three layered air-sea ice-sea water system, we assume a horizontal electric dipole as the excitation source. The source is placed on the sea ice surface. To measure field components, we choose the z component of the decoupled E and H fields as the necessary TM and TE field data. E_z will be measured along the endfire direction, and H_z will be measured along the broadside direction [19]. The expressions of the two fields are given below [44]:

$$\vec{E}_z^{TM} = \int_{-\infty}^{\infty} i\frac{Il}{8\pi\omega\epsilon_0}\left[k_\rho^2\left(1-\widetilde{R}_{0,1}^1\right)e^{ik_z z}H_1^{(1)}\left(k_\rho\rho\right)\cos\phi\right]dk_\rho \tag{6}$$

$$\vec{H}_z^{TE} = \int_{-\infty}^{\infty} i\frac{Il}{8\pi}\left[\frac{k_\rho^2}{k_z}\left(1+\widetilde{R}_{0,1}^2\right)e^{ik_z z}H_1^{(1)}\left(k_\rho\rho\right)\sin\phi\right]dk_\rho \tag{7}$$

Here, ρ is the radial distance from the source to the receiver, and ϕ is the azimuth angle which defines the radiation direction ($\phi = 0$ is the endfire direction, and $\phi = \frac{\pi}{2}$ is the broadside direction). I and l are the driving current and arm length of the dipole, respectively, and $\omega = 2\pi f$ is the frequency of operation. k_ρ is the tangential component of the dipole radiation, $k_z = k_{z,0}$ the propagation component along the direction of stratification, and z the height of the receiver. We refer to [20, 44] for the description of each term and will not elaborate in this article.

The dataset consists of "train features" and "target values". The train features include the electric and magnetic field values at defined receiver distance from the source, and the target values are the concerned thickness and dielectric properties of the sea ice bulk. There are also some "complimentary features" such as the temperature and salinities of the sea ice and sea water media, which are required to generate the dielectric properties of the three layered systems but not used to train the deep learning models. The arrangement of the dataset in tabular form is presented in Fig. 4.

The training features are generated over a range of frequencies as shown in Table 1 so that the model can learn the frequency dependent dielectric and loss tangent properties. Furthermore, it allows us to check the performance of the model when the test frequency is inside and outside the training frequency bands; therefore, we can evaluate the frequency adaptation of the trained model. If the performance of the model is acceptable outside the training bands, we can use a narrow band training data and apply the model over a wide range of frequencies. On the other hand, if the test features work only inside the training range, we need to train a larger model using a wide band training data.

Table 1. Ranges of each parameter to generate different air-sea ice-sea water environments. $[a, b]$ is a close interval ranging from a to b.

Ranges of data for field generation	Fixed		scaled	
	Analytical	FEM	Analytical	FEM
Frequency (MHz)	[2, 5]	[2, 5]	[2, 5]	[2, 5]
Temperature of sea ice (°C)	[−35, −10]	[−35, −15]	[−35, −10]	[−35, −15]
Temperature of sea water (°C)	[2, 8]	[2, 5]	[2, 8]	[2, 5]
Salinity of sea ice (ppm)	[2.2, 5.16]	[2.2, 5.16]	[2.2, 5.16]	[2.2, 5.16]
Salinity of sea water (ppm)	[6.4, 25.2]	[6.4, 25.2]	[6.4, 25.2]	[6.4, 25.2]
Thickness of sea ice (d) (m)	[0.5, 7]	[0.5, 7]	-	-
d/λ of sea ice	-	-	[0.05, 0.1]	[0.05, 0.1]
Receiver height (z) (m)	2	2	-	-
z/λ height	-	-	0.05	0.05
Receiver distance from the source (ρ) (m)	[3, 15]	[3, 15]	-	-
ρ/λ distance from the source	-	-	[0.01, 0.05]	[0.01, 0.05]
Number of measurement data point	122	42	68	22
Number of data samples	142740	2688	315120	8568

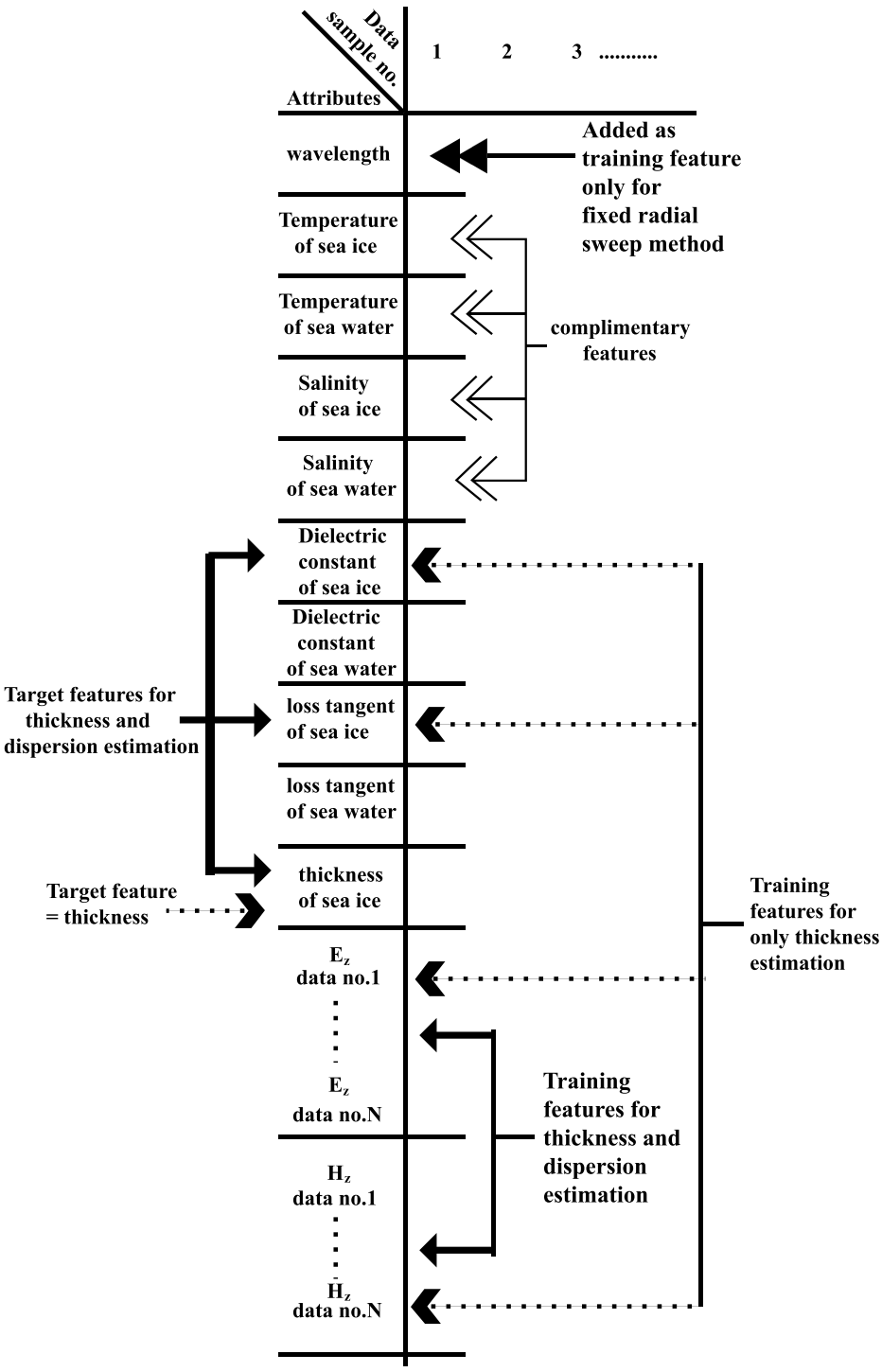

Figure 4. Attributes of the data samples used to solve the inverse problem. The left arrows point to the training features, and the right arrows point to the target values. The solid arrows represent the attributes used to estimate both dispersion and thickness of sea ice. The dotted arrows correspond to attributes when estimating thickness of sea ice only. The four double arrows pointed to the left denote the complimentary features, which are neither used for training nor as targets. The wavelength is used as an additional training feature for the fixed radial sweep method. N is the number of data along the measurement direction for the choice of radial sweep.

First, to generate the data, we needed to determine the height of the receiver and the spatial range across which the receiver dipole will be moved to capture the field data. We followed two approaches:

- In the first method, the height of the receiver and the spatial range of measurement with respect to the source dipole remain constant. We term this method of measurement as "Fixed radial sweep" of the receiver. The thickness of the sea ice layer is assumed to be within 1 m to 6 m, which is the typical thickness of the ice samples in the polar region [43]. We have chosen the receiver height to be 2 m, and the sweep distance of the receiver is set from 3 m to 15 m. Both of them are empirical choices. We have also chosen the wavelength (λ) of the excitation source as one of the training features for fixed radial sweep, as adding wavelength as an additional feature improves the performance of the deep learning network.
- In the second approach, measurement distance and receiver height were scaled with respect to the wavelength. We term the method of measurement as "Scaled radial sweep" of the receiver. The receiver distance from the source was varied from 0.01λ to 0.05λ, and the height was fixed at 0.05λ for each operating frequency. For the scaled radial sweep method, the wavelength is removed from the training features; as all the parameters are scaled with respect to wavelength, and the structures are frequency independent, the wavelength would add no additional information. We also note that removing wavelength from the training features slightly improves the performance of the training model.

When we try to measure the thickness and dispersion curves beyond the training frequency range, we expect that the scaled radial sweep method would perform better than the fixed sweep method. Because the former method enables us to get an approximately wavelength-independent representation of the field values, where the receiver distance, height, and measured thickness are scaled to the wavelength, and the only frequency-dependent variant is the dispersion relation embedded in the reflection coefficients (the derivation is provided in Appendix A). The concept is further explained in Fig. 5, where the training frequency range and extrapolated test frequency ranges are specified on the dispersion curves obtained from experimental data. The curves are somewhat exponential and monotonically decreasing in all the three specified ranges, and therefore, the model trained on the middle range should be able to extrapolate the prediction outside the training frequency boundary.

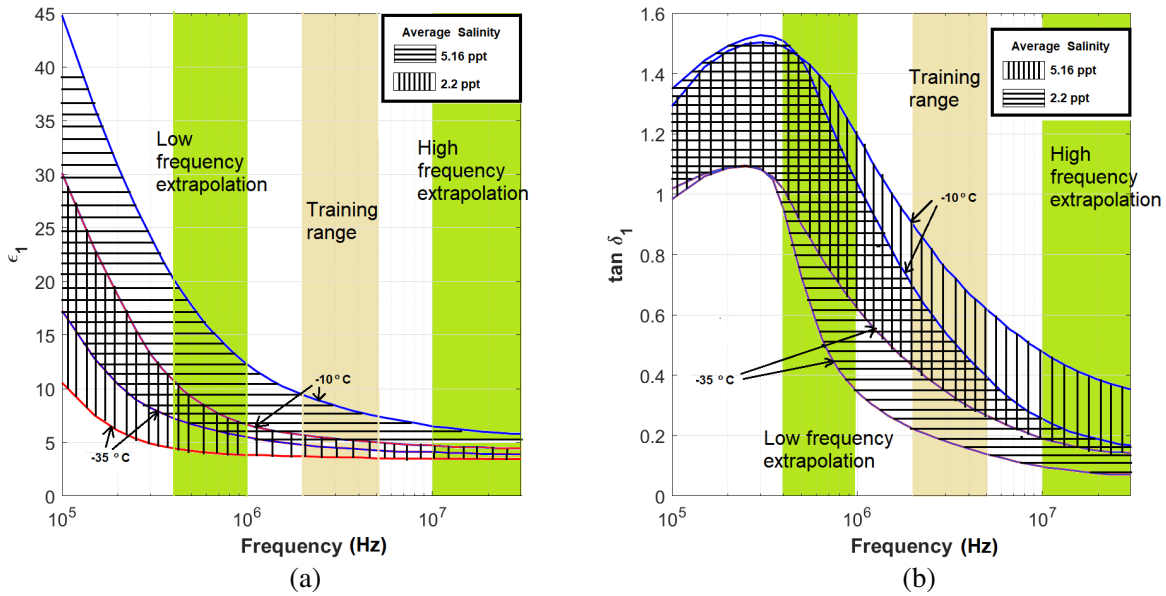

Figure 5. Extrapolation of the dispersion curves of sea ice outside the training bounds: (a) extrapolation of dielectric constant, (b) extrapolation of the loss tangent. The dispersion curves are taken directly from [33].

3.3. Description of the Deep Learning Model

As for the deep learning model, we have chosen a simple three layered multilayer perceptron (MLP) for mapping the input features into target values. For the fixed radial sweep, the input layer consists of the wavelength and the magnitude of the field values. For the scaled radial sweep, only the field magnitudes are used in the input layer. The field data are normalized using standard Z-score normalization. When we try to estimate both the thickness and the dielectric properties, the output layer includes ϵ_1, $\tan\delta_1$, and d. When we examine the performance of the model to estimate the thickness only, ϵ_1 and $\tan\delta_1$ are used as input features, and only d is used as output value.

The structure of the deep learning network is shown in Fig. 6. The intermediate layers are a series of three fully connected layers, with 512, 1024, and 2048 nodes respectively at each layer. Each layer is nonlinearized using the ReLu activation. The final layer, or the output layer, has no activation function as the outputs are regressive.

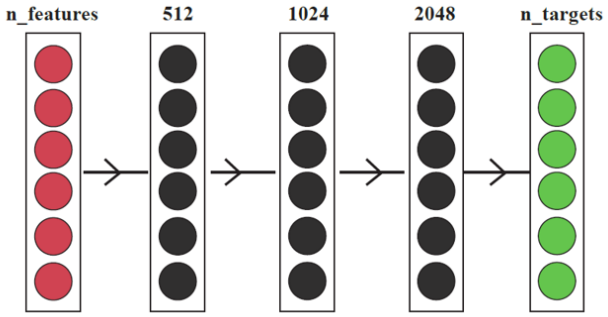

(a)

Measurement Method	Estimation parameters	n_features	n_targets
Fixed radial sweep	$\epsilon_{c,1}$, d	$1+2m$	3
	d	$3+2m$	1
Scaled radial sweep	$\epsilon_{c,1}$, d	$2p$	3
	d	$2+2p$	1

(b)

Figure 6. (a) Architecture of the deep learning model for solving the inverse problem. (b) The number of input features and output values for different measurement methods and estimation parameters. Here, m is the number of electric/magnetic field measurement points for fixed radial sweep and p is the number of electric/magnetic field measurement points for scaled radial sweep.

Since the inverse problem of solving the thickness and the dielectric constants from the field data is a regression problem, we use mean squared error (MSE) as the main loss function to update the parameters of the model. As for the optimizer, Adam optimizer has been defined, with an initial learning rate of 0.001. The training data are divided into an $8:2$ train to validation set, and the batch size is set to 16. In order to tackle overfitting, the learning rate is reduced at each plateau, and the epoch count stopped after sufficient epoch count failed to improve the validation loss.

4. RESULTS

In this section, we present the performance of the deep learning network to solve the inverse problem of estimating the thickness and dielectric properties of sea ice on different test datasets. For the performance evaluation, we have defined the mean absolute percentage error (MAPE) as the evaluation metric, which is defined as follows:

$$\text{MAPE} = \frac{1}{N}\sum_{n}\left|\frac{\text{actual\_value}(n) - \text{predicted\_value}(n)}{\text{actual\_value}(n)}\right| \times 100\%$$

where $N = \sum n$.

We first observe that the model learns very well with the analytical dataset. Figs. 7(a) and 7(b) show the training and validation loss curves for this dataset. We see that the validation loss is quite low for both fixed and scaled radial sweeps, and there is no sign of overfitting. To the contrary, training with the FEM dataset results in higher validation loss, as can be seen in Figs. 7(a) and 7(d). There is some overfitting to the training dataset due to the small number of FEM data.

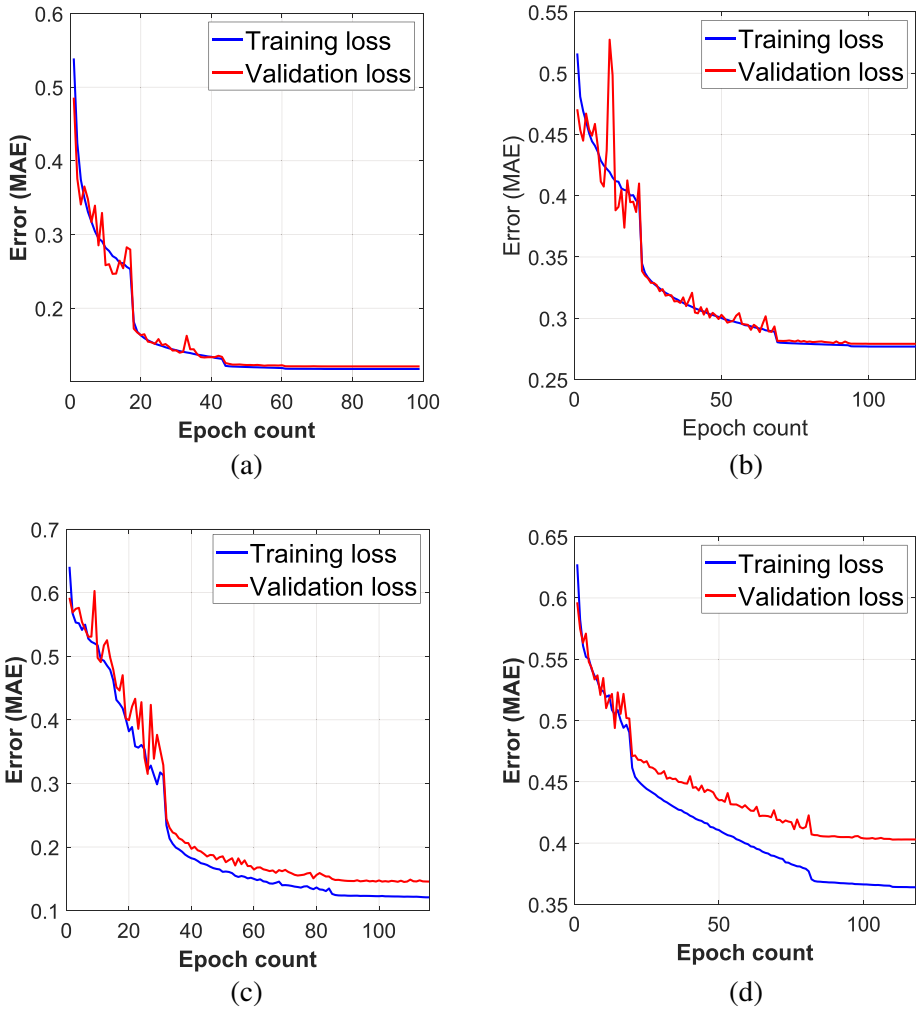

Figure 7. Training and validation loss curves of the deep learning model for different methods of training. (a) Fixed radial sweep with analytical data, (b) scaled radial sweep with analytical data, (c) fixed radial sweep using FEM model, (d) scaled radial sweep using FEM model.

4.1. Simultaneous Characterization of Sea Ice

Now we present the performance of our model for simultaneous characterization of sea ice using fixed and scaled radial sweep methods. We also show whether a set of training data with a defined frequency band can be used to interpolate at different measurement frequencies.

4.1.1. Fixed Radial Sweep

Figure 8(a) describes the efficacy of the model to solve the inverse problem for fixed radial sweep measurements. From the analytical test sets, we can see that when the test dataset's frequency is in the frequency range of the training set, the percentage error of ϵ_1 is always less than 2%, the $\tan\delta_1$ error less than 10%, and the thickness error less than 5%. This suggests that the simultaneous estimation of all three parameters is indeed possible with a high degree of accuracy. However, for this method, if the measurement frequency is even slightly outside the training range, performance of the model degrades very rapidly. The error on d deteriorates the fastest, while errors on ϵ_1 and $\tan\delta_1$ degrade more gradually. Therefore, it can be said that the fixed radial sweep measurement is not capable of frequency domain adaptation, but a very viable method to solve the inverse problem provided the measurement data is within the training range.

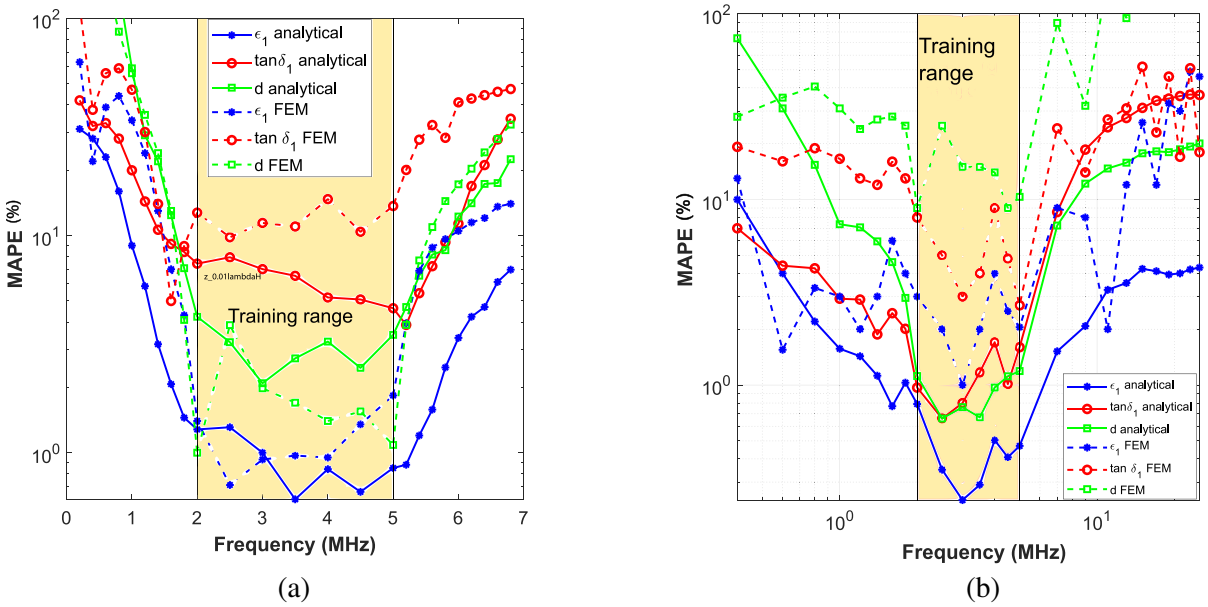

Figure 8. Estimation error (MAPE) of ϵ_1, $\tan\delta_1$ and d for the test dataset at different measurement frequencies: (a) fixed radial sweep, (b) scaled radial sweep.

4.1.2. Scaled Radial Sweep

Figure 8(b) shows the performance of the model when we take the scaled approach to solve the problem. We notice that when the measurement frequency is inside the training limits, ϵ_1, $\tan\delta_1$ and d errors for analytical dataset are less than 1%, which is a significant improvement compared to the fixed radial sweep. The performance degradation for test frequencies outside the training limits is also gradual, and even for frequencies as high and low by a factor of 5, we see that the estimation error is less than 10% for ϵ_1 and $\tan\delta_1$, and less than 20% for d.

Though the scaled radial sweep performs better than the fixed radial sweep, the gradual increase of error indicates that the model is not capable of completely learning the dispersion relations of the sea ice and sea water models outside the training limits. The intertwined relation between the thickness and the dielectric properties as mentioned in Section 2 may cause an estimation error.

On the contrary, the fixed radial sweep fails even when the test frequency is slightly outside the training frequency range. This is because if we keep the receiver height fixed, then it would imply different $\frac{z}{\lambda}$ ratios for each frequency of measurement. This results in completely different patterns of field magnitudes which is difficult to learn by the model.

Comparing the analytical results with the FEM estimations, we do see some degradation of quality for the latter. Specially, for the scaled sweep method, the improvement in performance is not so obvious. This can be attributed to the fact that the FEM model could not generate data identical to the analytical data, as well as the insufficient amount of FEM data used for the training, which resulted in a quick overfitting of the model.

4.2. Estimation of Sea Ice Thickness

Finally, we have chosen to test the performance of our deep neural network in determining the thickness only, assuming ϵ_1 and $\tan\delta_1$ are known a priori. In this case, the ϵ_1 and $\tan\delta_1$ values are passed to the deep learning network as training features, and the thickness d remains the only target to be estimated. Now the thickness measurement error, as shown in Fig. 9, has improved drastically over all the ranges of test frequency for both the fixed and variable sweep methods. We can see that the error is close to 0% inside the training frequency range, and it is less than 20% outside the training frequency range. However, a noticeable error still persists when FEM data are considered.

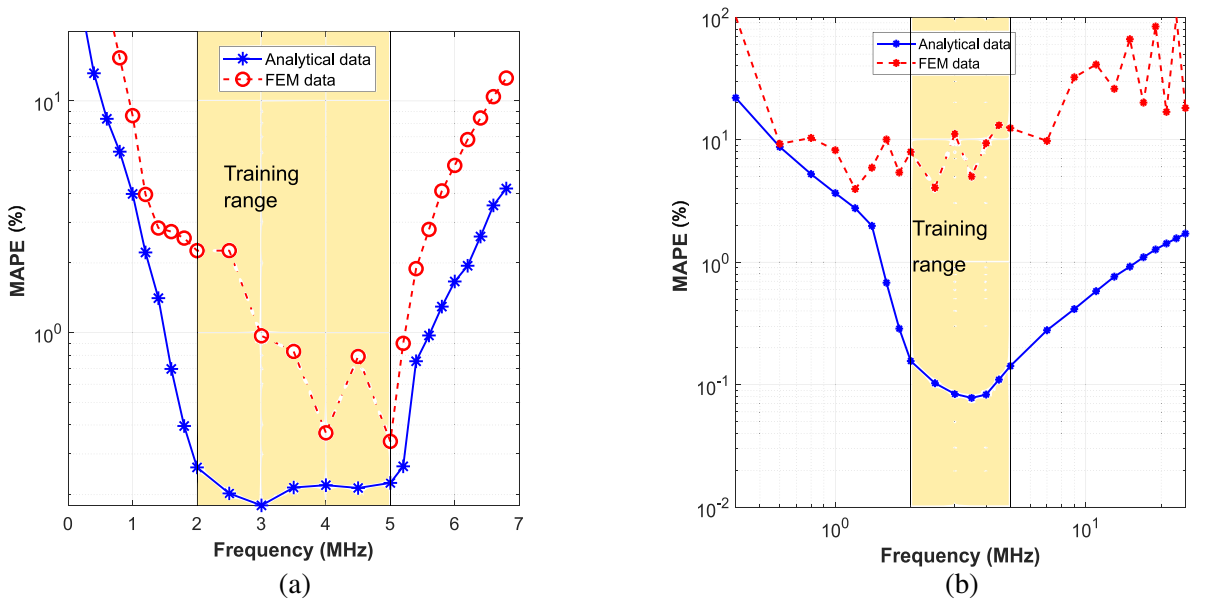

Figure 9. Estimation error (MAPE) of determining the sea ice thickness using a priori dielectric information: (a) fixed radial sweep, (b) scaled radial sweep.

5. CONCLUSION

In this work, we have examined multiple schemes of thickness and dielectric estimation of sea ice over seawater. Deep learning models trained on both analytical and FEM data show good measurement accuracy with low estimation error. For example, when we simultaneously estimate the thickness and dielectric parameters, the error is $< 1\%$. The error goes down as low as 0.1%, when we estimate thickness utilizing the priori knowledge of the dielectric parameters. For practical use case and the most accurate evaluation of this method, extensive physical measurements and data acquisition will be necessary. While we believe that a thorough demonstration and the feasibility has been presented, there is also significant scope for improvements. Instead of using the "analytically efficient" dipole antennas, there is definite possibility of developing more complex antenna systems, which would radiate more along the stratification layers and capture stronger field responses. The one-dimensionality of the radial sweep does poses a strict practical limitation that the receiver height to wavelength ratio must always be nearly constant, and this practical aspect of the problem could/may be circumvented using more elaborated 2D and 3D mapping over multiple receiver location. Overall, this work provides a baseline methodology to simultaneously estimate the thickness and dispersion characteristics of sea ice, and the performance of the proposed method is already very encouraging. Branching out further research and undertaking steps for practical experiments would improve this baseline, which is a part of further work.

ACKNOWLEDGMENT

This work has been supported by the Office of Naval Research Global, London, UK [grant N62909-19-1-2013] as part of the NICOP project "Non-invasive measurement of sea ice thickness using low frequency EM waves". The formal report of the project is available in [50].

APPENDIX A. WAVELENGTH NORMALIZED REPRESENTATION OF THE FIELD VALUES

Let the receiver distance, height, and thickness of the sea ice be expressed as a constant scaling factors of wavelength, i.e., $\rho = c_1\lambda$, $z = c_2\lambda$ and $d = c_3\lambda$. Since the wave propagation constant $k = \frac{2\pi}{\lambda}$, the

tangential component $k_\rho = \frac{2\pi}{\lambda}\sin\theta$, and the component along propagation $k_z = \frac{2\pi}{\lambda}\cos\theta$, from Section 2 we can write $k_\rho\rho = 2\pi c_1 \sin\theta$, $k_z z = 2\pi c_2 \cos\theta$ and $g(\sqrt{\epsilon_{c,1}}d) = 2ik_{z,1}d = 4i\pi c_3\sqrt{\epsilon_{c,1}}$. Substituting these values to Equation (4) we get:

$$\widetilde{R^j_{0,1}} = \frac{f_j(\sqrt{\epsilon_{c,1}}) + e^{4i\pi c_3\sqrt{\epsilon_{c,1}}\pm i\pi}}{1 + f_j(\sqrt{\epsilon_{c,1}})e^{4i\pi c_3\sqrt{\epsilon_{c,1}}\pm i\pi}} = \widetilde{R_j}(\epsilon_{c,1}, c_3) \tag{A1}$$

with $j = 1, 2$ representing TM or TE reflection. Considering free space (where $\omega = kc$, c being the speed of wave propagation) and modifying (6) we find:

$$\begin{aligned} E_z^{TM} &= K_1 \int_{-\infty}^{\infty} \left(\frac{2\pi}{\lambda}\right)^2 \sin^2\theta \left(1 - \widetilde{R_1}(\epsilon_{c,1}, c_3)\right) e^{2\pi i c_2 \cos\theta} \cdot H_1^1(2\pi c_1 \sin\theta)\cos\phi\cos\theta d\theta \\ &\propto \frac{1}{\lambda^2}\int_{-\infty}^{\infty} \left(1 - \widetilde{R_1}(\epsilon_{c,1}, c_3)\right) e^{2\pi i c_2\cos\theta} H_1^1(2\pi c_1\sin\theta)\cdot\sin^2\theta\cos\theta\cos\phi d\theta \end{aligned} \tag{A2}$$

where $K_1 = \frac{iIl}{8\pi c\epsilon_0}$. Since c_1, c_2, and c_3 are all constant terms, and the only frequency-dependent term is $\widetilde{R_1}(\epsilon_{c,1}, c_3)$, the values of E_z^{TM} during the radial sweep become weakly dependent on frequency. Similarly, it can be shown from (7) that the normalized H_z^{TE} is also weakly dependent on the frequency:

$$H_z^{TE} \propto \frac{1}{\lambda^2}\int_{-\infty}^{\infty} \left(1 + \widetilde{R_2}(\epsilon_{c,1}, c_3)\right) e^{2\pi i c_2\cos\theta} H_1^1(2\pi c_1\sin\theta)\cdot\sin^2\theta\cos\theta\sin\phi d\theta \tag{A3}$$

REFERENCES

1. Annan, A. P., "Radio interferometry depth sounding: Part I — Theoretical discussion," *Geophysics*, Vol. 38, No. 3, 557–580, Jun. 1973. [Online]. Available: https://doi.org/10.1190/1.1440360.
2. Rossiter, J. R., G. A. LaTorraca, A. P. Annan, D. W. Strangway, and G. Simmons, "Radio interferometry depth sounding: Part II — Experimental results," *Geophysics*, Vol. 38, No. 3, 581–599, Jun. 1973.
3. Tsang, L., J. A. Kong, and G. Simmons, "Interference patterns of a horizontal electric dipole over layered dielectric media," *Journal of Geophysical Research (1896–1977)*, Vol. 78, No. 17, 3287–3300, Jun. 1973. [Online]. Available: https://agupubs.onlinelibrary.wiley.com/doi/abs/10.1029/JB078i017p03287.
4. Liao, D. H. and K. Sarabandi, "Near-earth wave propagation characteristics of electric dipole in presence of vegetation or snow layer," *IEEE Transactions on Antennas and Propagation*, Vol. 53, No. 11, 3747–3756, Nov. 2005.
5. Kong, J., "Electromagnetic fields due to dipole antennas over stratified anisotropic media," *Geophysics*, Vol. 37, No. 6, 985–996, 1972.
6. Chew, W. C. and J. A. Kong, "Electromagnetic field of a dipole on a two-layer Earth," *Geophysics*, Vol. 46, No. 3, 309–315, Mar. 1981.
7. Lee, J., A. J. Park, Y. Tanabe, A. S. Poon, and S. Kim, "A microwave method to remotely assess the abdominal fat thickness," *AIP Advances*, Vol. 11, No. 3, 035111, 2021.
8. Shah, S. R. M., N. B. Asan, J. Velander, J. Ebrahimizadeh, M. D. Perez, V. Mattsson, T. Blokhuis, and R. Augustine, "Analysis of thickness variation in biological tissues using microwave sensors for health monitoring applications," *IEEE Access*, Vol. 7, 156 033–156 043, 2019.
9. Scharfetter, H., T. Schlager, R. Stollberger, R. Felsberger, H. Hutten, and H. Hinghofer-Szalkay, "Assessing abdominal fatness with local bioimpedance analysis: Basics and experimental findings," *International Journal of Obesity*, Vol. 25, No. 4, 502–511, 2001.
10. Donelli, M., "A rescue radar system for the detection of victims trapped under rubble based on the independent component analysis algorithm," *Progress In Electromagnetics Research M*, Vol. 19, 173–181, 2011.

11. Pasolli, E., F. Melgani, M. Donelli, R. Attoui, and M. De Vos, "Automatic detection and classification of buried objects in GPR images using genetic algorithms and support vector machines," *IGARSS 2008 — 2008 IEEE International Geoscience and Remote Sensing Symposium*, Vol. 2, II–525, IEEE, 2008.
12. Pasolli, E., F. Melgani, and M. Donelli, "Gaussian process approach to buried object size estimation in GPR images," *IEEE Geoscience and Remote Sensing Letters*, Vol. 7, No. 1, 141–145, 2009.
13. Alibakhshikenari, M., B. S. Virdee, C. H. See, R. A. Abd-Alhameed, F. Falcone, and E. Limiti, "Super-wide impedance bandwidth planar antenna for microwave and millimeter-wave applications," *Sensors*, Vol. 19, No. 10, 2306, 2019.
14. Alibakhshikenari, M., B. S. Virdee, C. H. See, P. Shukla, S. Salekzamankhani, R. A. Abd-Alhameed, F. Falcone, and E. Limiti, "Study on improvement of the performance parameters of a novel 0.41–0.47 THz on-chip antenna based on metasurface concept realized on 50 µm GAAS-layer," *Scientific Reports*, Vol. 10, No. 1, 11034, 2020.
15. Altaf, A., A. Iqbal, A. Smida, J. Smida, A. A. Althuwayb, S. Hassan Kiani, M. Alibakhshikenari, F. Falcone, and E. Limiti, "Isolation improvement in UWB-MIMO antenna system using slotted stub," *Electronics*, Vol. 9, No. 10, 1582, 2020.
16. Alibakhshikenari, M., B. S. Virdee, P. Shukla, Y. Wang, L. Azpilicueta, M. Naser-Moghadasi, C. H. See, I. Elfergani, C. Zebiri, R. A. Abd-Alhameed, et al., "Impedance bandwidth improvement of a planar antenna based on metamaterial-inspired T-matching network," *IEEE Access*, Vol. 9, 67 916–67 927, 2021.
17. Kiourti, A., C. W. Lee, J. Chae, and J. L. Volakis, "A wireless fully passive neural recording device for unobtrusive neuropotential monitoring," *IEEE Transactions on Biomedical Engineering*, Vol. 63, No. 1, 131–137, 2015.
18. Lee, C. W., A. Kiourti, and J. L. Volakis, "Miniaturized fully passive brain implant for wireless neuropotential acquisition," *IEEE Antennas and Wireless Propagation Letters*, Vol. 16, 645–648, 2016.
19. Balanis, C. A., *Antenna Theory: Analysis and Design*, John Wiley & Sons, 2015.
20. Islam, M. S., S. Shafi, M. I. Hasan, and M. A. Haque, "Low frequency near field interferometry for characterization of lossy dielectric and an investigation on sea ice," *IEEE Transactions on Geoscience and Remote Sensing (Early Access)*, 1–11, 2020.
21. Trentini, G. V., "Partially reflecting sheet arrays," *IRE Transactions on Antennas and Propagation*, Vol. 4, No. 4, 666–671, 1956.
22. Islam, M. S., S. Shafi, and M. A. Haque, "Development of an experimental model of low frequency dipole radiation in the presence of multilayered structures," *SoutheastCon 2021*, 1–6, IEEE, 2021.
23. Chollet, F., *Deep Learning with Python*, Simon and Schuster, 2021.
24. Heaton, J., "Ian Goodfellow, Yoshua Bengio, and Aaron Courville: Deep learning," *Genetic Programming and Evolvable Machines*, Vol. 19, 305–307, 2018.
25. Gao, Y., H. Liu, X. Wang, and K. Zhang, "On an artificial neural network for inverse scattering problems," *Journal of Computational Physics*, Vol. 448, 110771, 2022.
26. Zhang, P., P. Meng, W. Yin, and H. Liu, "A neural network method for time-dependent inverse source problem with limited-aperture data," *Journal of Computational and Applied Mathematics*, Vol. 421, 114842, 2023.
27. Yin, W., W. Yang, and H. Liu, "A neural network scheme for recovering scattering obstacles with limited phaseless far-field data," *Journal of Computational Physics*, Vol. 417, 109594, 2020.
28. Yin, W., J. Ge, P. Meng, and F. Qu, "A neural network method for the inverse scattering problem of impenetrable cavities," *Electronic Research Archive*, Vol. 28, No. 2, 1123–1142, 2020.
29. Islam, M. S., S. Shafi, and M. A. Haque, "Low-frequency electromagnetic characterization of layered media using deep neural network," *2021 International Symposium on Antennas and Propagation (ISAP)*, 1–2, IEEE, 2021.
30. Stogryn, A., "Equations for calculating the dielectric constant of saline water (correspondence)," *IEEE Transactions on Microwave Theory and Techniques*, Vol. 19, No. 8, 733–736, 1971.

31. Addison, J. R., "Electrical properties of saline ice," *Journal of Applied Physics*, Vol. 40, No. 8, 3105–3114, 1969.
32. Stogryn, A., "An analysis of the tensor dielectnc constant of sea ice at microwave frequencies," *IEEE Transactions on Geoscience and Remote Sensing*, No. 2, 147–158, 1987.
33. Wentworth, F. and M. Cohn, "Electrical properties of sea ice at 0.1 to 30 mc/s," *J. Res. NBS*, Vol. 68, 681–691, 1964.
34. Evans, S., "Dielectric properties of ice and snow — A review," *Journal of Glaciology*, Vol. 5, No. 42, 773–792, 1965.
35. Buchanan, S., M. Ingham, and G. Gouws, "The low frequency electrical properties of sea ice," *Journal of Applied Physics*, Vol. 110, No. 7, 074908, 2011.
36. Hallikainen, M. and D. P. Winebrenner, "The physical basis for sea ice remote sensing," *Washington DC American Geophysical Union Geophysical Monograph Series*, Vol. 68, 29–46, 1992.
37. Holt, B., P. Kanagaratnam, S. P. Gogineni, V. C. Ramasami, A. Mahoney, and V. Lytle, "Sea ice thickness measurements by ultrawideband penetrating radar: First results," *Cold Regions Science and Technology*, Vol. 55, No. 1, 33–46, 2009.
38. Tilling, R. L., A. Ridout, and A. Shepherd, "Estimating arctic sea ice thickness and volume using cryosat-2 radar altimeter data," *Advances in Space Research*, Vol. 62, No. 6, 1203–1225, 2018, The CryoSat Satellite Altimetry Mission: Eight Years of Scientific Exploitation. [Online]. Available: https://www.sciencedirect.com/science/article/pii/S0273117717307901.
39. Lindsay, R. and A. Schweiger, "Arctic sea ice thickness loss determined using subsurface, aircraft, and satellite observations," *The Cryosphere*, Vol. 9, No. 1, 269–283, 2015.
40. Schanda, E., *Physical Fundamentals of Remote Sensing*, Springer Science & Business Media, 2012.
41. Bourke, R. H. and R. P. Garrett, "Sea ice thickness distribution in the arctic ocean," *Cold Regions Science and Technology*, Vol. 13, No. 3, 259–280, 1987.
42. Eicken, H., W. Tucker, and D. Perovich, "Indirect measurements of the mass balance of summer arctic sea ice with an electromagnetic induction technique," *Annals of Glaciology*, Vol. 33, 194–200, 2001.
43. Thomas, D. and G. Dieckmann, *Sea Ice*, 2nd Edition, Wiley-Blackwell, Jan. 2010.
44. Chew, W., *Waves and Fields in Inhomogeneous Media*, Springer, 1990.
45. Cheng, D. K., *Field and Wave Electromagnetics*, Pearson Education, India, 1989.
46. Wait, J. R., A. Cullen, V. Fock, J. Wait, and H. Hagger, "Electromagnetic waves in stratified media," *Physics Today*, Vol. 17, No. 4, 76, 1964.
47. Jackson, J. D., *Classical Electrodynamics*, 1999.
48. Inc., C., "Comsol," 2020. [Online]. Available: http://www.comsol.com/products/multiphysics/.
49. Klein, L. and C. Swift, "An improved model for the dielectric constant of sea water at microwave frequencies," *IEEE Transactions on Antennas and Propagation*, Vol. 25, No. 1, 104–111, 1977.
50. Haque, M. A., M. S. Islam, S. Shafi, M. Hasan, et al., "Non-invasive measurement of sea ice thickness using low frequency EM waves," *Anyeshan Limited, Tech. Rep.*, 2022.